Engineering Structures 60 (2014) 265–275

Contents lists available at ScienceDirect

Engineering Structures

journal homepage: www.elsevier.com/locate/engstruct

Natural frequencies identification of a reinforced concrete beam using carbon nanotube cement-based sensors

Filippo Ubertini [a,*], Annibale Luigi Materazzi [a], Antonella D'Alessandro [a], Simon Laflamme [b,c]

[a] Department of Civil and Environmental Engineering, University of Perugia, Perugia, Italy
[b] Department of Civil, Construction, and Environmental Engineering, Iowa State University, Ames, IA 50011, USA
[c] Department of Electrical and Computer Engineering, Iowa State University, Ames, IA 50011, USA

ARTICLE INFO

Article history:
Received 23 July 2013
Revised 17 December 2013
Accepted 28 December 2013
Available online 25 January 2014

Keywords:
Smart concrete
Nanotechnology
Carbon nanotubes
Cement-based transducers
Multifunctional materials
Concrete structures
Operational modal analysis
Structural health monitoring

ABSTRACT

Cementitious materials doped with carbon nanoparticles are robust materials capable of transducing strain into changes in electrical resistance. These properties encourage the development of spatially distributed sensors for structural health monitoring of concrete structures. Yet, very few applications of transducers made of cement-based nanocomposites to structural elements have been documented. The majority of applications are limited to measurement of static responses.

The authors have recently proposed the novel application of cement-based nanocomposite technologies for vibration-based structural health monitoring of concrete structures. To this aim, prismatic sensors made of cement paste doped with carbon nanotubes have been proposed as embedded sensors for concrete structures. Prior results have shown the promise of these sensors at vibration measurements. In this paper, the authors further the understanding of the dynamic behavior of cement-based carbon nanotube sensors by conducting experiments on a full-scale reinforced concrete beam for output-only identification of natural frequencies. The performance of the novel sensor is benchmarked against off-the-shelf strain gauges and accelerometers. Results show that the proposed sensor compares well against existing technologies at vibration monitoring. Also, the nanocomposite sensor is capable of detecting high frequencies, which is made possible by a very low level of noise and an excellent signal-to-noise ratio obtained from shielded wire connections and proper tailoring of the fabrication process.

© 2014 Elsevier Ltd. All rights reserved.

1. Introduction

Continuous assessment of structural health through vibration measurements has become one of the key issues of structural health monitoring (SHM). This online monitoring is typically conducted through an automated investigation of modal parameters estimates and of their temporal variations [1,2], using multivariate statistical analysis tools [3]. Recent field applications of continuous vibration-based monitoring include long-span bridges [4], footbridges [5] and historic structures [6].

It is recognized that SHM of civil structures has the potential to enable timely inspection and maintenance, consequently enhancing structural safety and structural life expectancy [7,8]. However, practical SHM applications are still limited. One factor impeding the wide applicability of SHM solutions is associated with the inherent size of the structures to be monitored. Most existing sensing solutions are hardly scalable without necessitating substantial costs and complex signal processing algorithms, making SHM financially unattractive to infrastructure owners due to their apparent low return on investment.

The rapid growth of nanotechnologies has opened new possibilities in sensor developments [9,10], including new multifunctional materials that enable substantial improvements in the cost-effectiveness of SHM solutions for geometrically large systems [11,12]. Building on these technological advances, the authors have recently developed a strain sensor fabricated from a multifunctional cement-based composite material, with the objective to provide an innovative solution to the large scale monitoring challenge of concrete structures.

The material consists of a self-sensing cement paste doped with carbon nanotubes [13]. The resulting sensor, termed carbon nanotube cement-based sensor (CNTCS), transduces local strain into a change in electrical resistance. CNTCSs can be applied over large linear segments or embedded prior to casting to enable monitoring of concrete structures. When embedded, CNTCS forms a mechanically strong bond with the monitored structure, and creates a continuously distributed set of strain sensors within the structure. CNTCS also have a durability similar to the structure, which allows long-term applications with limited maintenance.

* Corresponding author. Tel.: +39 075 585 3954; fax: +39 075 585 3897.
E-mail address: filippo.ubertini@unipg.it (F. Ubertini).

0141-0296/$ - see front matter © 2014 Elsevier Ltd. All rights reserved.
http://dx.doi.org/10.1016/j.engstruct.2013.12.036

In a prior work [13], the authors investigated the electrical response of CNTCS when subjected to sinusoidal compression loads at various frequencies. Although only a limited frequency range was investigated (up to 5 Hz), results suggested that CNTCSs were promising at dynamic measurements, and encouraged more extensive investigations devoted to assessing their performances at vibration-based SHM.

In this paper, the authors further the understanding of CNTCS by examining its capability to perform output-only modal identification. This verification is conducted through laboratory vibration tests on a reinforced concrete (RC) beam, where a significantly larger range of frequencies is investigated in comparison to prior work. For the first time, the performance of the CNTCS is benchmarked against mature, off-the-shelf sensors. Also, efforts are made to enhance the CNTCS signal-to-noise ratio to improve the resolution in dynamic identification. These include modifications to the fabrication process and to the data acquisition procedures.

The paper is organized as follows. Section 2 presents the background theory on CNTCS, including the state-of-the-art summary, fabrication process, and sensing principle. The sensor's improvements in comparison to prior work are discussed. Section 3 describes the methodology used for dynamic identification of a full-scale concrete beam through CNTCS. A discussion on the improvements in the data acquisition procedure is provided. Section 4 shows and discusses the experimental results. Section 5 concludes the paper.

2. Description of nanotube cement-based sensors

2.1. State-of-the-art summary

Earliest studies on self-sensing cementitious materials appeared in the 90s [14]. The physical principle of strain sensing in these materials is based on a change in their electrical resistivity. A strain in the materials provokes a change in piezoresistivity caused by the slight pull-out of the fibers passing through microcracks [15]. This occurs if the nanoparticles are properly dispersed in the matrix and their amount reaches a critical fraction termed *percolation threshold*.

Following these first publications on multifunctional cement-based composites, different dopants have been investigated, including carbon fibers [15,16], nanocarbon black [17] and, more recently, carbon nanotubes (CNTs) [18,19]. It has been shown that CNTs possess excellent electrical and mechanical properties, which are now exploited in different types of nanocomposites (e.g. [20]). While these properties make CNTs promising dopants, their dispersion within the cementitious matrix is significantly complicated by their low solubility in water solutions [21]. In particular, the development of appropriate physical and chemical procedures is necessary to produce bundle-free three-dimensional CNTs networks.

In sensing applications, the vast majority of literature has focused on the static response of nanotechnology-modified cement-based materials, while vibration-based SHM has been almost unexplored. The authors have developed the CNTCS, specifically tailored to dynamic measurements. For this purpose, the fabrication process of CTNCS has been refined to optimize the sensitivity. This refinement includes enhanced physical and chemical methods for dispersing the CNTs to obtain an homogeneous composite material. Unlike traditional strain gauges, CNTCS are fabricated with a cementitious material, which allows embeddement within an external cover of concrete structures and provides a strong mechanical bond. This results in a life expectancy of the sensing hardware similar to the one of the monitored structure, and opens the possibility to cost-effectively monitor large structural surfaces via a continuous distributed sensor network.

The following subsections describe the CNTCS physical properties, its fabrication process, and the sensing principle.

2.2. Physical properties of CNTCS

The specimens fabricated for the experimental campaign consist of square-base prisms made of nanomodified cementitious material with embedded electrodes.

The specimens dimensions are $40 \times 40 \times 160\ mm^3$. The electrodes consist of copper wires of 1 mm diameter, disposed symmetrically with respect to the center of the specimens, equally spaced at a distance of 10 mm and embedded in approximately 3/4 of the width of the specimens. Eight electrodes are embedded with the purpose of allowing measurements in different configurations (e.g. two-probe, four-probe, etc.), with various distances between active electrodes.

The matrix of the CNTCS consists of a cement paste fabricated with Portland cement type 42.5 and a water/cement ratio of 0.40. This material provides a suitable homogeneity and enhances strain sensitivity in comparison to mortar or concrete. Conductive nanoparticles are dispersed in the matrix, consisting of multi walled carbon nanotubes (MWCNTs) type Graphistrength C100 from Arkema. The particular structure of MWCNTs, made of concentric cylinders of graphene sheets, makes them more sensitive than Single Walled CNTs. The physical properties of the particular MWCNTs selected in the fabrication process are reported in Table 1. The composite material mix design is summarized in Table 2, also reporting quantities used for a single specimen.

2.3. Fabrication process

The fabrication process of CNTCS is schematically described in Fig. 1. First, a Sky 521 plasticizer based on second-generation polycarboxylate ether polymers is added to deionized water at a concentration of 5% by volume of water (Fig. 1(a)). Second, MWCNTs are added to the mix in the amount of 2% by weight content of cement (Fig. 1(b)). Since nanotubes are not hydrophile, a specific sequence of mixing processes with different devices is adopted to disperse the MWCNTs within the mix before the addition of cement powder. This dispersion technique aims at preventing CNTs from agglomerating into bundles, which would result in a lack of homogeneity in the composite material, and is conducted as follows. The MWCNTs solution is first mixed with a magnetic stirrer for 10 min (Fig. 1(c)). It is followed by 15 min of sonication with a 225 W ultrasound device equipped with a probe series Vibra Cell Bioblock Scientific model 75043. (Fig. 1(d)). During sonication the beaker containing the nanomodified solution is soaked in a cool water bath, in order to limit evaporation. Lastly, the solution is mixed for 15 min with a mechanical agitator with a speed of rotation of 1500 rev/min (Fig. 1(e)). Sonication has been recognized as the key step in the manufacturing process, which mostly affects strain sensitivity of CNTCS. For this reason, the duration of the

Table 1
Physical properties of the MWCNTs used in the experiment.

Property	Description/Value
Appearance	Black powder
Apparent density	50–150 kg/m^3
Mean agglomerate size	200–500 μm
Weight loss at 105 °C	<1%
Carbon content	>90% in weight
Free amorphous carbon	Undetectable (SEM)
Mean number of walls	5–15
Outer mean diameter	10–15 nm
Length	0.1–10 μm

Table 2
Cement paste mix design.

Components	Content/m^3	Content/specimen
MWCNTs	32.4 kg	8.3 g
Portland cement 42.5	1620 kg	415 g
Superplasticizer	32.4 dm^3	8.3 cm^3
Water	650 kg	166 g
w/c	0.4	0.4

whole dispersion process is increased from 15 to 40 min in comparison to prior work [13], with a longer sonication time.

The nanomodified aqueous solution resulting from the mixing procedure is added to cement powder (Fig. 1(f)), and manually mixed to obtain the nanocomposite cement paste. The material is then poured into oiled molds (Fig. 1(g)) and the copper electrodes are embedded in the paste (Fig. 1(h)). After settling, the sample is unmolded for curing (Fig. 1(i)).

The effective dispersion of nanoparticles in the aqueous solution and in the cement paste is controlled using a scanning electron microscope (SEM) (type FESEM, model Supra 25, Zeiss) with a field emission cathode. SEM analyses are reported in Fig. 2(a) for the water solution with MWCNT after the mixing procedure and in Fig. 2(b) for a fragment of hardened nanocomposite cement paste. Both figures demonstrate the good dispersion of nanotubes and the effectiveness of the mixing process.

2.4. Sensing principle

The resulting CNTCS is a strain transducer. A strain in the cementitious materials (or even a crack) alters the contact between the nanoparticles, which in turn changes the materials electrical resistivity, which can be measured via a data acquisition system. The relation between incremental variation in electrical resistance, ΔR, measured by CNTCS and the variation in axial strain, $\Delta\epsilon$, is written:

$$\frac{\Delta R}{R_0(t)} = \lambda(\epsilon, \dot{\epsilon})\Delta\epsilon \tag{1}$$

where R_0 is the unstrained electrical resistance and λ is a gauge factor. Unlike for conventional strain gauges, Eq. (1) is nonlinear as λ depends on the axial strain ϵ as well as on the strain rate $\dot{\epsilon}$ [19]. This dependance of λ on ϵ is explained by a closer interaction between nanoparticles following an applied stress, while its dependency with $\dot{\epsilon}$ is due to specific electrical behavior of the composite material. Literature suggests that the electrical behavior of the sensor could be modeled at a first level of approximation by a resistor and a capacitor in parallel with some contact resistance [22]. The capacitor is used to model the rate dependency of λ. Also, due to the presence of non-negligible electrical capacitance in the sensor, its electrical response and, consequently, its unstrained electrical resistance, R_0, vary with time because of the material polarization under the application of a constant electrical field.

Remark: from Eq. (1), the sensitivity of the CNTCS, $\Delta R/\Delta\epsilon$, is proportional to R_0. While an increase in the content of nanoparticles would result in a larger λ, it would also provoke an overall decrease in the sensitivity of the sensor. It follows that an optimal content of nanoparticles exists. For the sensor described in this section, this optimal content is approximately 2% by weight of cement. A side effect of an increase in R_0 is the increase in the power voltage necessary to obtain a measurable level of current intensity.

In this paper, linearity of Eq. (1) is assumed for output-only frequency identification. As it will be demonstrated in the experiments, this assumption is justified by the observation that natural frequencies of vibration can be identified from standard spectral analysis of CNTCS's output, as it is commonly done with linear transducers.

3. Experimental procedures

3.1. Experimental setup

The laboratory setup comprises (see Fig. 3): (i) a simply supported RC beam; (ii) carbon-nanotube cement-based sensors, off-the-shelf accelerometers, an impulse hammer, and electric strain gauges; (iii) a chassis for data acquisition with five slots; (iv) a power source module for providing stabilized electrical input to the CNTCS; (v) a digital multimeter module for measuring the electrical response of the CNTCS; (vi) a data acquisition module and A/D converter for strain gauges; and (vii) a data acquisition module and A/D converter for accelerometers and impulse hammer. These components are described in what follows.

The RC beam has a total length of 430 cm and a rectangular cross-section of dimensions 20×30 cm^2. The beam is equipped with two steel plates partially embedded at its extremities prior to casting serving as vertical supports. The plates are inserted into steel supports to allow end rotations in the vertical plane while fixing rotations in the horizontal plane. The distance between the supports is 400 cm. Longitudinal and transverse steel reinforcements of the RC beam are shown in Fig. 3.

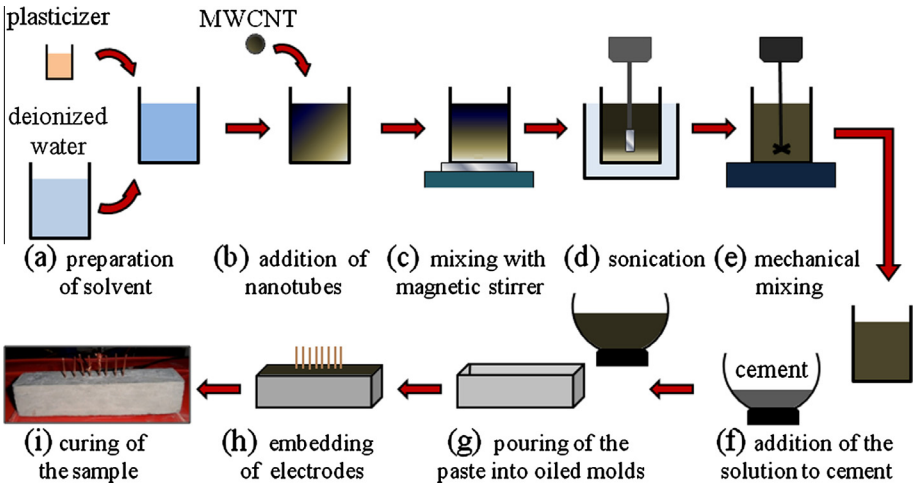

Fig. 1. Fabrication process of a CNTCS.

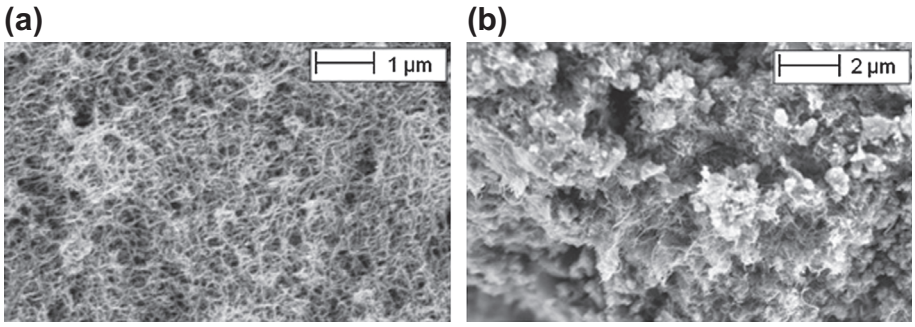

Fig. 2. SEM pictures of the CNTCS: (a) water suspension with CNTs; and (b) hardened composite cement paste.

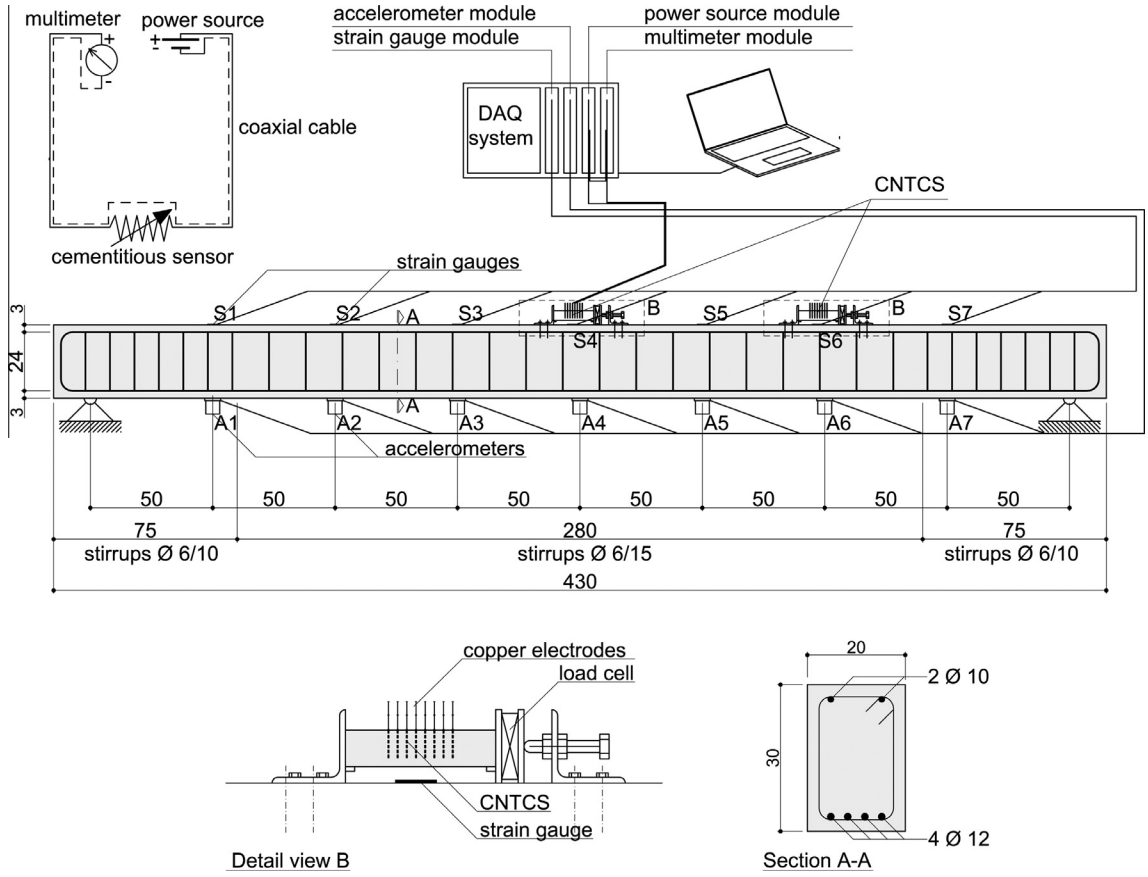

Fig. 3. Layout of the experimental setup and plans of the investigated RC beam (dimensions in cm).

CNTCS, described in Section 2, are attached on the top surface of the RC beam at mid- and quarter-span by means of mechanical connection devices. Each connection device is made from two L-shaped steel elements each one connected to the RC beam by four bolts. A screw is installed in one of the two L-shaped elements to apply an initial prestress to the sensor, whose level is manually adjusted using a load cell with a digital display. This prestress is used to simulate embedment. The sensors are electrically isolated from the connection devices using thin plastic sheets.

Seven equally spaced seismic accelerometers are mounted on the bottom of the RC beam to measure its vertical vibrations. Accelerometers (model PCB393C) have a sensitivity of 1 V/g, measurement range of ±2.5 g, and have a frequency range of 0.025–800 Hz with associated dynamic error of ±5%. They are wired to the central unit by means of short coaxial cables, and attached through permanent magnets on 4×4 cm steel bases, 0.8 cm thick, which are glued on the beam. Seven electric strain gauges for concrete (model KC-60-120-A1-11-L1M2R) are attached at the same locations of the accelerometers, but on the top concrete surface of the beam. These strain gauges have vinyl-coated flat 2-wire cable, gage factor of 2.1, length of 60 mm and a nominal electric resistance of 120 Ω.

The data acquisition chassis is a NI PXIe-1073 and hosts four modules: one for power source generation, one for measuring the electrical output of the cementitious sensors, one for acquisition and A/D conversion of the signals provided by the strain gauges, and one for acquisition and A/D conversion of the signals provided by the accelerometers. The chassis is connected to a PC, model Dell Latitude E6530, through the NI Express card interface. A Labview code is developed to simultaneously manage power generation

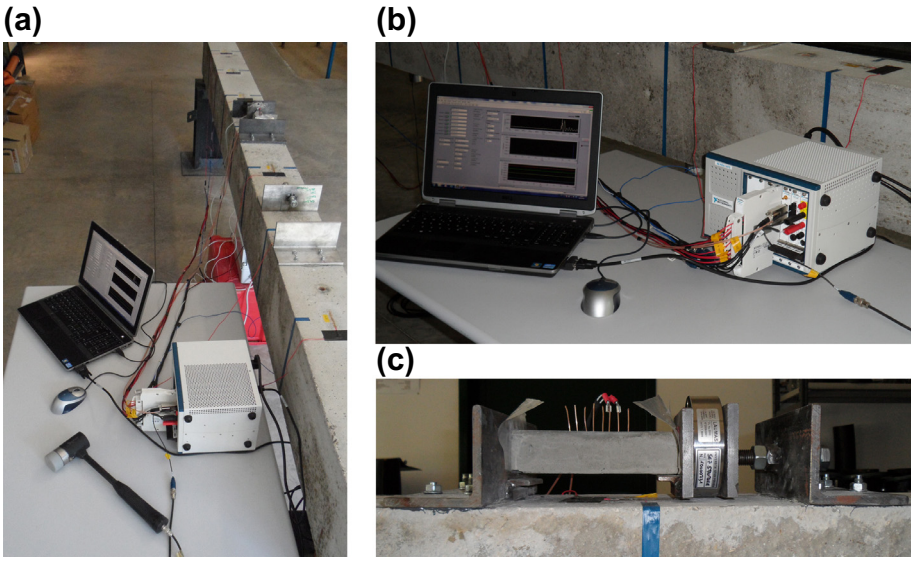

Fig. 4. Experimental setup: overview (a); hardware for power source generation and data acquisition (b); CNTCS mounted on the RC beam (c).

and signal acquisitions from the different sensors. The stabilized potential difference sent to the CNTCS is provided by a NI PXI-4130 capable of providing a four-quadrant ±20 V and ±2 A output in a single isolated channel.

The high speed digital multimeter, model NI PXI-4071, is also installed in the chassis and used to perform electrical measurements. The module allows voltage, current and electrical resistance measurements. The current measurement range used for the experiment is ±100 μA with resolution of 100 pA ±1 pA. An 18-bit A/D conversion is used with a sampling rate tuned to 1 kHz.

The impulse hammer used for the dynamic excitation, model PCB 086*D*20*C*41 with ICP quartz force sensor, has a 0.23 mV/N sensitivity and ±22,240 N measurement range.

Strain gauges measurements are acquired through a data acquisition bridge input module, model PXIe-4330, 8 channels, 24-bit resolution, 25 kHz maximum sampling rate, anti-aliasing filters. The accelerometers and hammer outputs are acquired through a data acquisition module, model PXIe-4492, 8 channels, 24-bit resolution, 204.8 kHz maximum sampling rate, anti aliasing filters.

The current intensity outputted by the CNTCS under application of a stabilized power voltage is measured, and the conversion to electrical resistance is performed by diving applied voltage by the measured current intensity. In order to minimize the electromagnetic interference with the high sampling rate, shielding is improved on the electrical circuit connecting power source unit, sensors and digital multimeter. This is done by means of a single coaxial cable, where the internal copper wire connects the positive probe of the multimeter, through the sensor, and to the positive pole of the power generator, while the mesh shield connects the negative probe of the multimeter, through the sensor, and to the negative pole of the power generator, as shown in Fig. 3. This improved shielded connection has shown substantial reduction in measurement noise.

In this laboratory setup, a two-probe measurement configuration is adopted providing good quality of the measurements. In this particular configuration, an increase in the distance between active electrodes results in increasing R_0 and decreasing the output current intensity level. Consequently, the strain sensitivity of the sensor is increased, and signal-to-noise ratio decreased. An optimal balance exists, and it depends on the sampling rate which directly affects accuracy of current measurements. With the sampling rate utilized in this setup (1 kHz), a distance of 10 mm between the electrodes has shown to provide a good balance.

3.2. Vibration tests

Vibration tests are conducted by exciting the RC beam using the impulse hammer. Hammer hits are random in space and time. The response of the beam is measured and recorded simultaneously with the CNTCS, accelerometers and strain gauges. The electrical current outputted by the cementitious sensors under application of a stabilized potential difference of 15 V between electrodes placed at a distance of 10 mm is measured by the multimeter. In the vibration tests, CNTCS are prestressed with compression loads equal to 1.5 kN and are subjected to a constant electrical field during 30 min prior to testing at a potential difference of 15 V to minimize the effects of polarization. Pictures of the experimental setup are shown in Fig. 4.

Six data acquisitions periods are performed, each one having a duration of 150 s, with the accelerometers placed in the vertical direction. This duration is limited by the memory of the digital multimeter. For the first three data acquisition periods, one CNTCS is placed at the mid-span of the beam, while for the remaining acquisition periods, the CNTCS is placed at quarter-span of the beam. Data processing is conducted by concatenating collected data in a single data set. A highpass filter is used on the CNTCS output above 10 Hz to eliminate residual polarization effects.

A second set of experiments with only accelerometers placed in the lateral direction is performed to identify the horizontal modal characteristics of the beam. Data are acquired over a period of 430 s in this case.

The natural frequencies f_n^v and f_n^h of vertical and lateral modes, respectively, are analytically computed using the vibration theory for continuous beams with simply supported (vertical) and fixed-fixed (lateral) boundary conditions. The characteristic equation for the natural frequencies of vertical modes is

$$\sin(\beta_n^v L) = 0 \tag{2}$$

and for lateral modes is

$$\cos(\beta_n^h L)\cosh(\beta_n^h L) = 1 \tag{3}$$

with

$$\beta_n^2 = 2\pi f_n \sqrt{\frac{\mu}{EI}} \tag{4}$$

where L is the span length, $\mu \cong 2500\ \mathrm{kg/m^3}$ the material density, $E \cong 30{,}000\ \mathrm{N/mm^2}$ the Young modulus of concrete, and I the

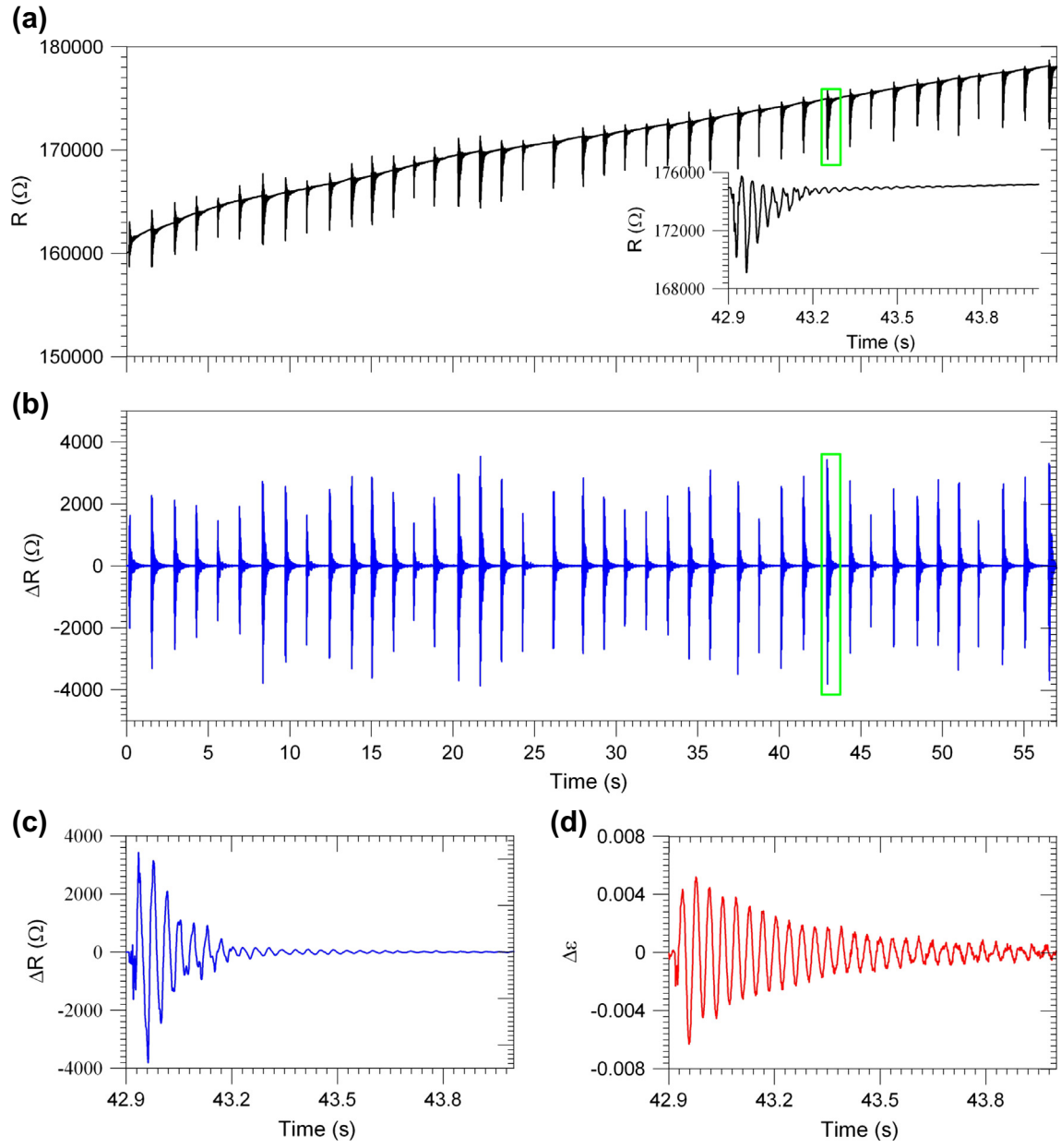

Fig. 5. Vibration monitoring of the RC beam using CNTCS placed at mid-span: sensor output before high-pass filtering (a); sensor output after high-pass filtering (b); blow up on sensor output (c); detailed window plot of the output of the strain gauge placed at the location of the CNTCS (d).

moment of inertia taken as $I^v = 200 \times 300^3/12$ mm^4 and $I^h = 300 \times 200^3/12$ mm^4 in vertical and lateral directions, respectively.

From Eq. (2), the analytical frequency for the first vertical mode is $f_1^v = 25.2$ Hz. From Eq. (3), the analytical frequency of the first lateral mode is $f_1^h = 38.1$.

Note that the data acquisition lengths largely satisfy the condition of being 1000–2000 times the fundamental natural period, which is necessary for performing an accurate output only modal identification.

3.3. Data processing techniques

The Choi-Williams time-frequency distribution is used for investigating the energy content of signals in the time-frequency domain. The choice of this mathematical tool is justified by its known robustness characteristics against noise and effectiveness in reducing interference terms [23].

Time-frequency distributions can be generalized as follows:

$$P(t,\omega) = \frac{1}{4\pi^2}\iint_{-\infty}^{+\infty} W(t-u)e^{-i\tau\omega}R_{\tau,1}(t,\tau)\mathrm{d}u\mathrm{d}\tau \tag{5}$$

where $W(t-u)$ is the Fourier transform of the Kernel function $\Phi(\theta,\tau)$ that acts as a filter of the local autocorrelation function $R_{\tau,1}(t,\tau) = x(u+\tau/2)x^*(u-\tau/2)$, $x(t)$ is the input signal, t denotes time, τ is a time lag parameter, $u = t+\tau/2$ and * denotes the complex conjugate operator. The inspection of Eq. (5) shows that the choice of the kernel function determines the characteristics of the time frequency distribution. The kernel function of the Choi-Williams distribution is defined as

$$\Phi(\theta,\tau) = e^{-\frac{\theta^2\tau^2}{\sigma}} \tag{6}$$

where σ is a user-defined scalar parameter. For more details on Choi-Williams distribution, the interested reader is referred to Ref. [23].

The modal parameters of the RC beam are extracted in the range of 0–500 Hz using the Frequency Domain Decomposition (FDD)

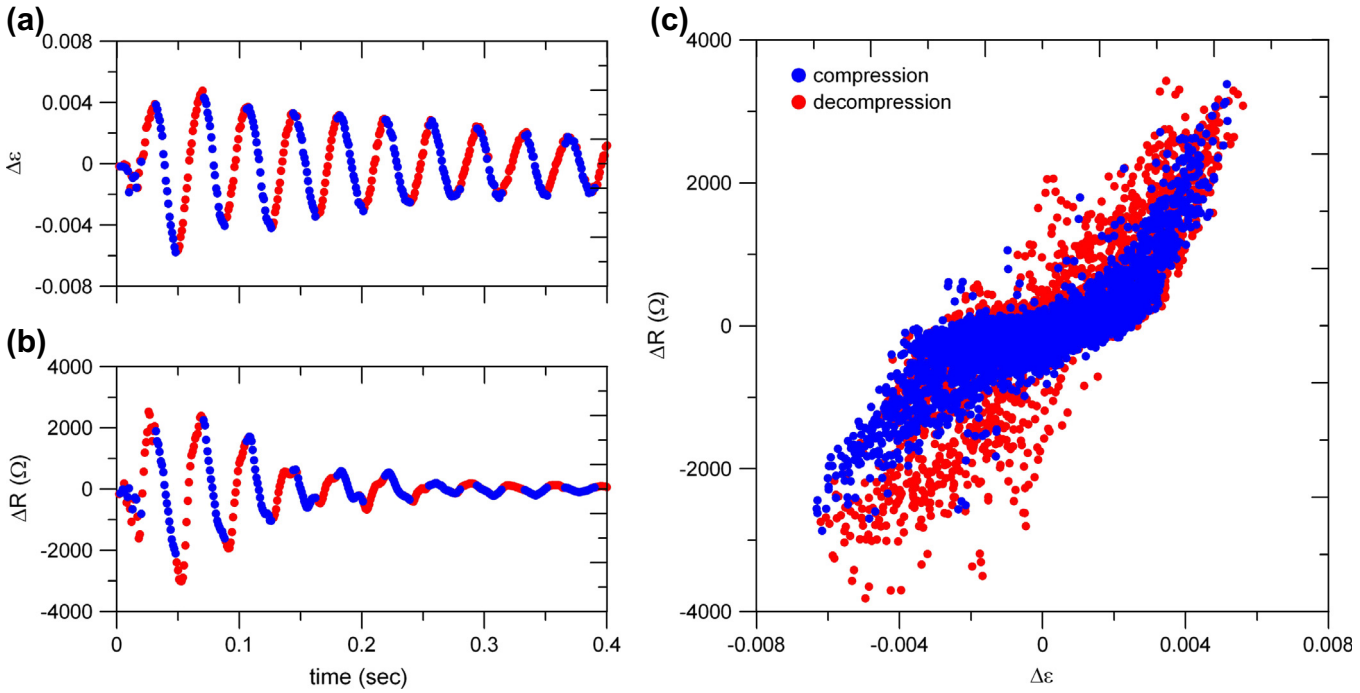

Fig. 6. Hysteretic behavior of the CNTCS: window plot of strain response at mid-span during hammer test (a); corresponding CNTCS output (b); CNTCS output vs. strain variation (c).

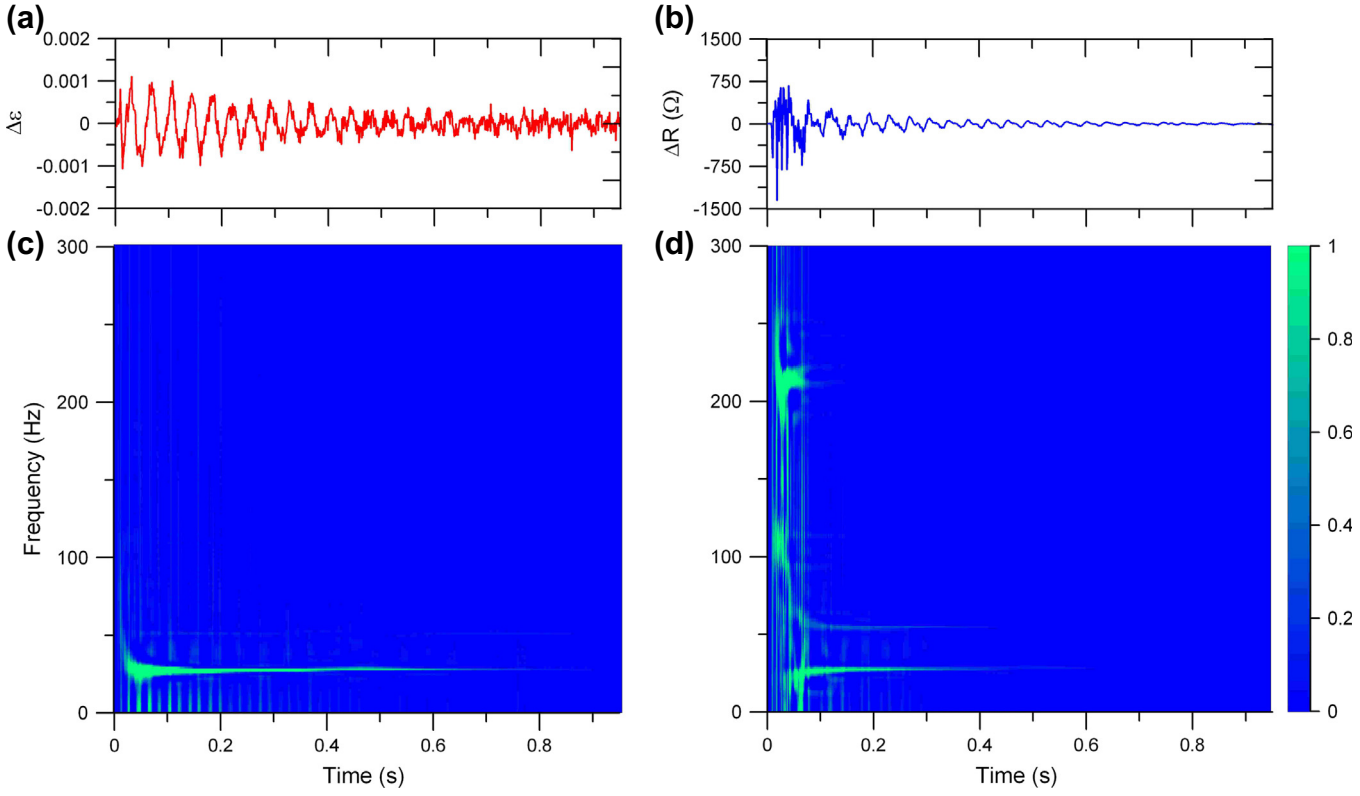

Fig. 7. Time-frequency analysis of strain measurement and corresponding CNTCS output at quarter-span: strain gauge output (a); CNTCS output (b); time-frequency plot of strain gauge output (c); time-frequency plot of CNTCS output (d).

method. The FDD is based on the evaluation of the matrix of cross-spectral densities of the output data $\mathbf{G}(f)$, where f denotes the frequency. Matrix $\mathbf{G}(f)$ contains the (real valued) auto-spectral densities along the main diagonal and the (complex) cross-spectral densities elsewhere. $\mathbf{G}(f)$ is computed by using the modified periodogram method yielding average spectra by subdividing the recorded signals into windows and overlapping frames containing 2^n points. This approach results in a frequency resolution equal to $f_s/2^{n+1}$, f_s being the sampling frequency. Modal parameters estimates are extracted from output data by decomposing matrix $\mathbf{G}(f)$

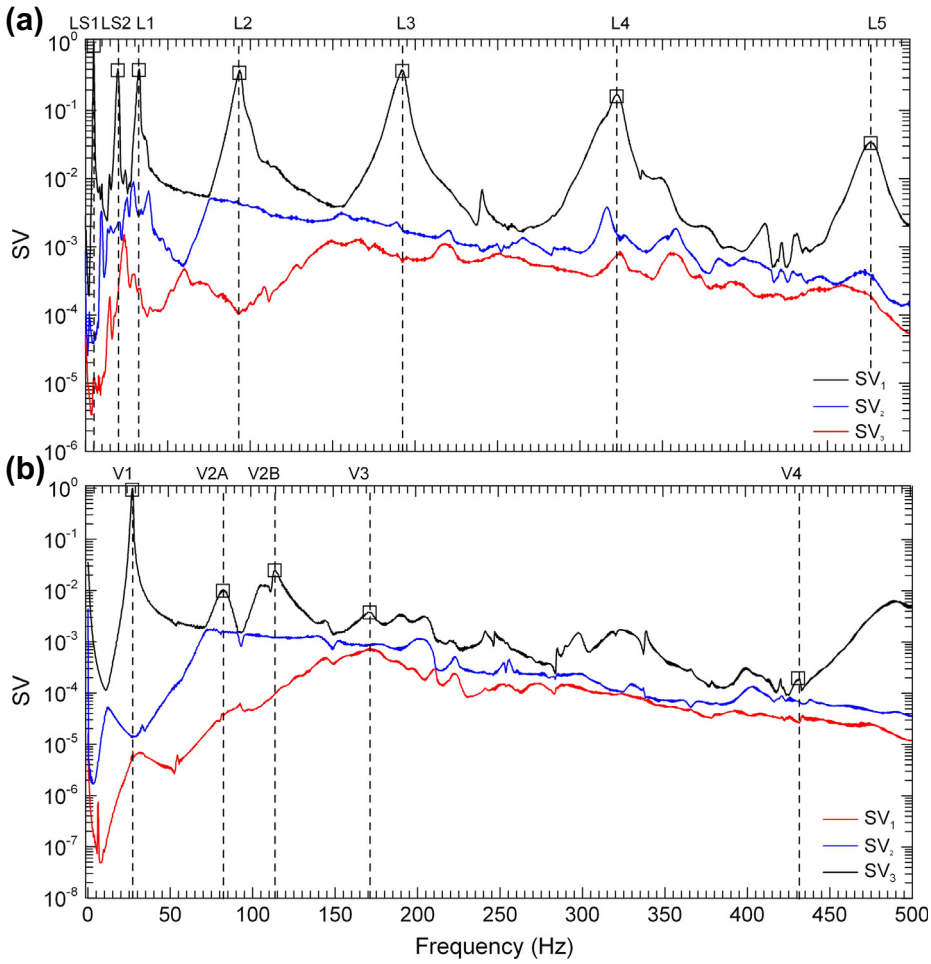

Fig. 8. Peaks and singular value lines of the data recorded by accelerometers placed in lateral (a) and vertical (b) directions.

through singular value decomposition at discrete frequencies. Assuming the input to be a white noise and damping to be small, natural frequencies are identified as those that correspond to the peaks of the curves representing the singular values of $\mathbf{G}(f)$. Mode shapes are approximated by taking the corresponding singular vectors.

4. Results and comparisons

4.1. Analysis of CNTCS outputs

Fig. 5(a) shows a time history of the data recorded from the CNTCS placed at mid-span during vibration tests. Hammer impacts can be recognized by the multiple peaks in the data. The signal exhibits a drift in the time domain. Examining the blow up of a single hammer hit response (shown in Fig. 5(a)), the signal is not symmetric around the steady state value, but mostly remains below. Both effects are conceivably associated to polarization. The time drift originates from a decrease in current intensity due to increasing charge in the dielectric material. The second effect is explained by a slow response to an impulsive compressive load superimposed to the dynamic response. As shown in Fig. 5(b), both effects are removed by a high-pass filter, but at the expense of low frequencies information.

A blow up on the response to a single hammer hit after filtering is shown in Fig. 5(c). The noise level of the signal is very low compared with literature on nanocomposite cement-based sensors. This demonstrates the success of the two major improvements in the sensing solution with respect to previous studies by the authors. First, the use of a coaxial cable in the electrical circuit connection to the CNTCS, power source, and multimeter (Fig. 3) has substantially reduced the electromagnetic noise. Second, the material preparation and type and position of active electrodes are optimized and contributed to improving the sensitivity of the transducer. Specifically, design for CNTCS in this work has resulted after comparison between different mix procedures, including the use of two types of dispersing additives (BYK 154 and BYK 190) and various distances between active electrodes. It was found that the use of dispersing additives can reduce unstrained electrical resistance R_0, Eq. (1), up to about one-third. Therefore, no dispersing additive is used here, but, in comparison with previous work [13], a longer sonication process is used for improving CNTs network. Fig. 5(a) shows a value for R_0 to be of the order of 170 kΩ. The signal-to-noise ratio achieved in the experiments allows to use sensor's outputs for output-only frequency identification in a wide frequency range.

Fig. 5(d) is a plot of a portion of signal measured by the strain gauge placed at the same location as the CNTCS. The comparison between Fig. 5(c) and (d) confirms the nonlinearity of Eq. (1): the CNTCS provides a signal which is quite evidently non-proportional to the one outputted by the strain gauge. An immediate consequence is a faster decay which prevents damping estimation from raw data recorded through the CNTCS.

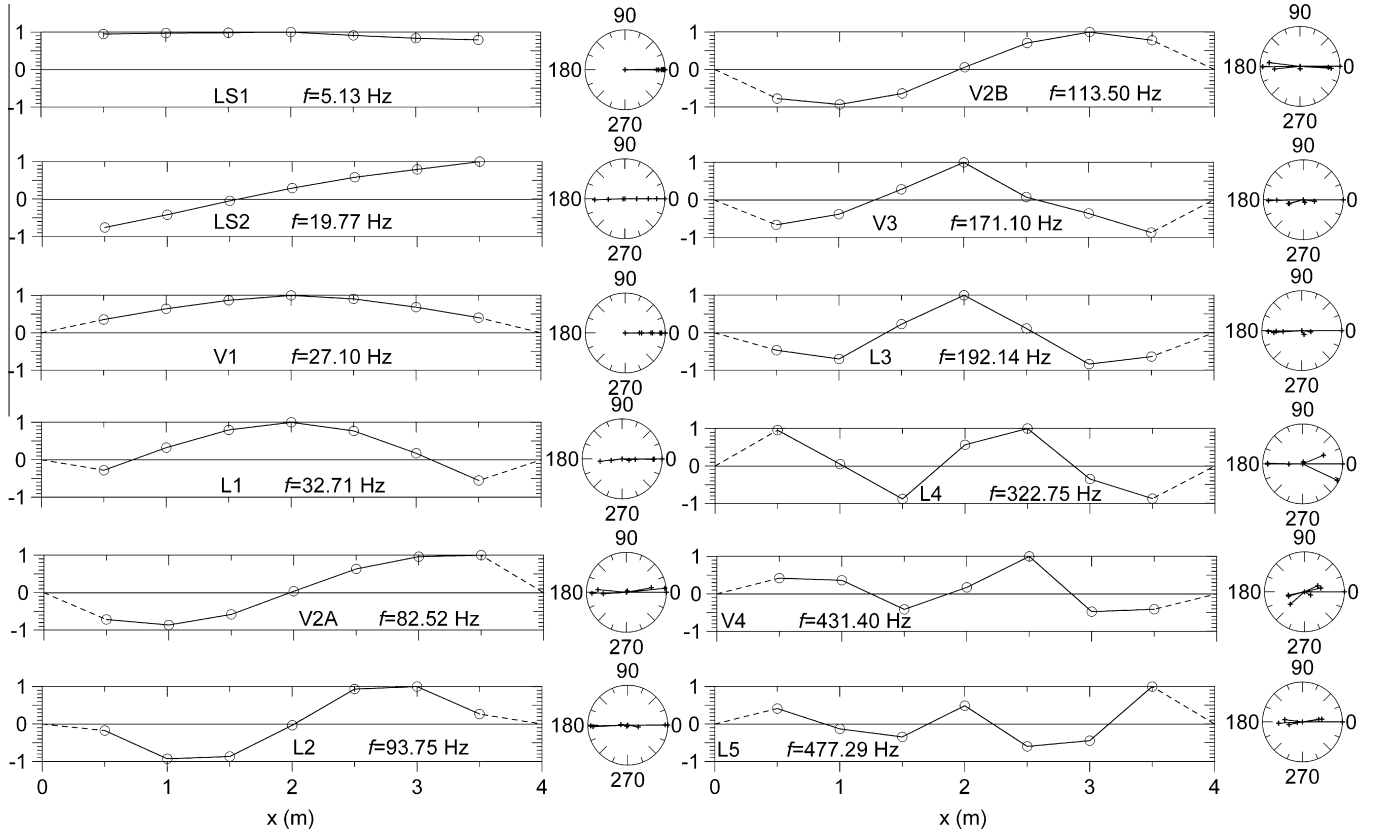

Fig. 9. Mode shapes identified using signals recorded by accelerometers and associated polar plots. Vertical and lateral modal components are shown in vertical and lateral modes, respectively.

Fig. 6(a) and (b) show the blow up of the CNTCS and strain gauge signals, in which compression and decompression are shown using different[1] colors. Fig. 6(c) is a plot of CNTCS output against strain gauge output for a longer period. These results show a hysteresis in the CNTCS response, with larger hysteresis during compression. No significant variation in sensitivity of the sensor with strain is observed, because the variations of strain with respect to the initial value from prestress force is relatively small.

Fig. 7 shows time-frequency plots in the range 0–300 Hz using the Choi-Williams distribution (Eq. (5)) for the CNTCS and strain gauge outputs placed at quarter-span. The signal from the strain gauge shows a single frequency around 27 Hz. The time-frequency plot of the strain gauge does not exhibit higher frequencies, because of a more significant level of noise in the measurements. The signal outputted by the CNTCS shows the same fundamental frequency around 27 Hz, with a much shorter decay time. The CNTCS exhibits higher frequency components. Significant energy of the signal is concentrated around 90 Hz, 110 Hz, and 220 Hz. As it will be shown in next section, some of these components (90 Hz and 110 Hz) are associated with vibration modes of the RC beam, while others (220 Hz) are spurious frequencies of uncertain origin, probably related to the non-white nature of the input. Some small amount of energy of the signal is also concentrated around 54 Hz. This spurious frequency is the double of the main frequency at 27 Hz, and could be a superharmonic component due to the harmonic distortion of the sensor's output caused by its nonlinearity.

[1] For interpretation of color in Fig. 6, the reader is referred to the web version of this article.

Table 3
Identified (ID) natural frequencies of the RC beam (Hz) using Frequency Domain Decomposition and traditional sensors (the relative difference, Δ, is calculated between analytical natural frequencies and frequencies identified from acceleration data).

Mode	Analytical	ID (accel.)	ID (strain g.)	Δ (%)
LS1	–	5.13	–	–
LS2	–	19.78	19.78	–
V1	25.22	27.10	27.10	7.4
L1	38.11	32.71	37.35	14.2
V2A	100.9	82.52	81.79	18.2
L2	105.1	93.75	93.75	10.8
V2B	100.9	113.5	113.5	12.5
V3	227.0	171.1	171.1	24.6
L3	206.0	192.1	192.6	6.7
L4	340.5	322.8	–	5.2
V4	403.5	431.4	–	6.9
L5	508.6	477.3	–	6.1

4.2. Identification of natural frequencies of the RC beam from CNTCS outputs

Fig. 8 shows the first three normalized singular value (SV) lines of the data recorded by the accelerometers placed in vertical (Fig. 8(a)) and lateral (Fig. 8(b)) directions. FDD results identify a total of 12 natural modes of vibration in the range between 0 and 500 Hz. These modes correspond to the peaks shown in Fig. 8. Identified modes are five vertical modes, denoted V1, V2A, V2B, V3 and V4, five lateral modes, denoted L1 to L5, and two additional lateral modes, denoted LS1 and LS2. The meaning of modes V2A and V2B will be clarified below. Identified mode shapes are reported in Fig. 9. Other peaks, visible in the SV plots of Fig. 8, are not associated to vibrational modes of the beam because their

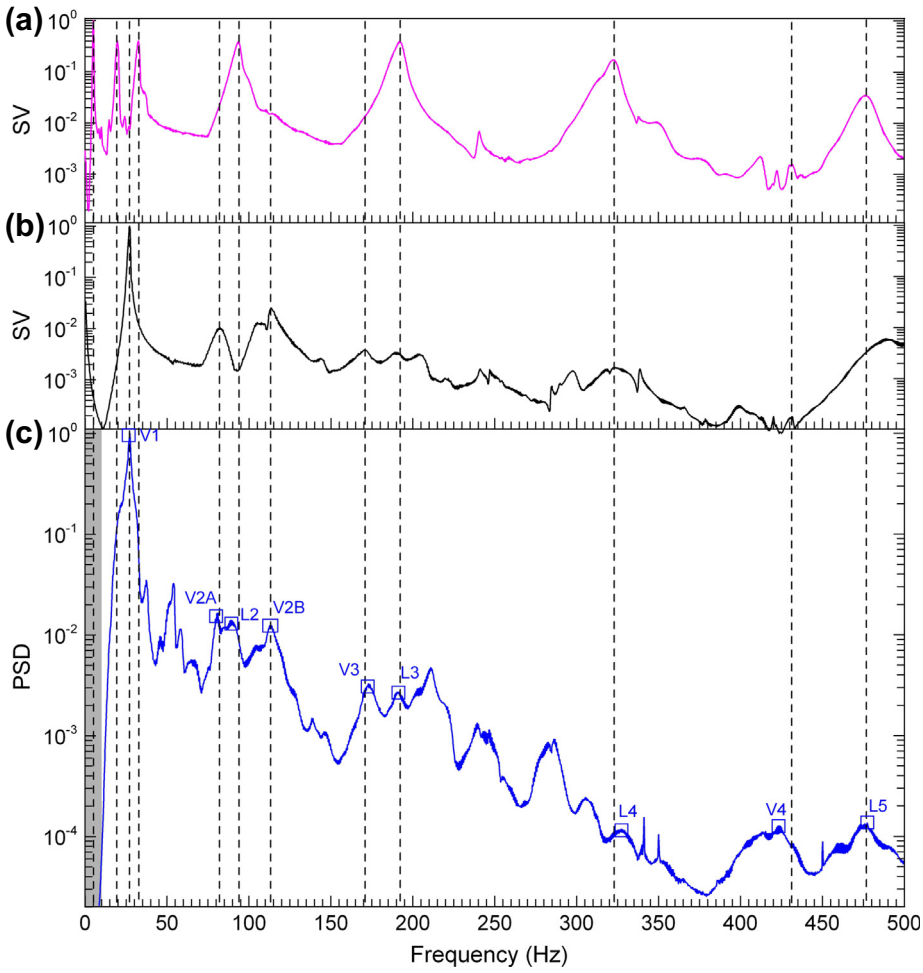

Fig. 10. Identification of natural frequencies with CNTCS: first normalized singular value of lateral acceleration data (a); first normalized singular value line of vertical acceleration data (b); peaks of the normalized PSD of the output of CNTCS (c) (the gray area denotes filtered region).

Table 4
Identified (ID) natural frequencies of the RC beam (Hz) using accelerometers and CNTCS.

Mode	V1	V2A	V2B	V3	V4
ID (accel.)	27.10	82.52	113.5	171.1	431.4
CNTCS	27.10	81.05	113.3	172.9	423.6
Δ (%)	0.0	1.8	0.2	1.0	1.8

corresponding eigenvectors are irregular and conceivably not corresponding to mode shapes of the beam. These peaks can be attributed to the non-white nature of the input in the vibration tests.

The comparison between identified and analytical frequencies is reported in Table 3. Results show a very good agreement for modes V1, V3, V4, L1, L2, L3, L4 and L5. Natural frequencies identified from data recorded using strain gauges are also reported in Table 3. Almost exact agreement exists with results from accelerometers. However, no clear peaks can be detected at frequencies higher than about 200 Hz due to a significant level of measurement noise.

The identified mode shapes are similar to theoretical modes from simply supported (vertical modes) and fixed-fixed (lateral modes) elastic beams. Two antisymmetric vertical modes, denoted as V2A and V2B, with very similar mode shapes are identified instead of a single mode V2. This is probably a splitting of the modal frequency, a phenomenon often documented in literature for damaged RC elements [24]. The RC beam under investigation was subject to artificial damage in previous work, consisting of deep cracks at mid-span.

Mode shapes LS1 and LS2 are associated with the rolling motion of the supports over their bases. In particular, mode LS1 involves in phase lateral motions of the supports, while mode LS2 involves out of phase lateral motions of the supports. These motions were visually observable during the experiments.

Fig. 10 shows the normalized power spectral density (PSD) of the data recorded from CNTCS and compared against the normalized first singular value lines of the spectral matrices of the acceleration measurements in the two (vertical and lateral) setups. Results show that all vertical modal peaks visible in the SV lines of acceleration data are also evident in the PSD of the CNTCS output. Although the CNTCS was expected to measure only vertical vibration, peaks related to lateral modes are also observable in its output spectrum. While the peak associated with mode LS1 is not visible because it falls into the filtered region, two bumps around the main peak of mode V1 are visible, which could be associated with modes LS2 and L1. The output spectrum of the CNTCS also shows the peaks associated to modes L2, L3, L4 and L5. The presence of the superharmonic peak associated to twice the frequency of mode V1 is evident in the PSD of the CNTCS output signal, and confirms to observation from Section 4.1 about the harmonic distortion characterizing the CNTCS.

The comparison between the frequencies of vertical modes identified through acceleration data and those corresponding to

the peaks of the output spectrum of the CNCTS is reported in Table 4. A similar comparison for lateral modes is not possible because the CNTCS was not placed in a position apt to accurately measure lateral vibrations. Results presented in Table 4 show that the frequencies identified from the peaks of the PSD function of the CNTCS output correspond to the vertical modal frequencies of the beam.

5. Conclusions

In this paper, the use of composite cementitious sensors with carbon-nanotubes has been proposed for vibration monitoring of RC structures. Prismatic transducers made of multifunctional strain-sensing cement paste doped with carbon nanotubes have been prepared with an optimized fabrication process to ameliorate the dispersion of MWCNTs. Vibration experiments covered a frequency range to an extent never investigated in previous work. The interest in measuring relatively high frequency responses is motivated by possible applications of cement-based sensors to relatively rigid structures, such as low-rise buildings and precast concrete girder bridges, as well as by possible applications of structural health monitoring techniques based on high frequency responses. Results from the experiments were benchmarked against mature, off-the-shelf accelerometers and strain gauges. Overall results have shown that the novel nanocomposite cement-based sensors are promising for output-only identification of natural frequencies, with significant advantages with respect to traditional sensors, including the possibility to build self-sensing structures equipped with an arbitrarily large number of durable sensors arranged in a network configuration. Specific conclusions of this work are as follows:

- The CNTCS outputs very small levels of current intensities, and thus requires the use of high precision multimeters for measurements. The tailored fabrication process of CNTCS resulted in an enhanced sensitivity associated to a high unstrained electrical resistance. Also, improved shielding of the electrical circuit connecting the sensor, data acquisition and power modules using a coaxial cable has almost eliminated electromagnetic noise, and enabled modal identification over a frequency range up to 500 Hz.
- CNTCS exhibit a non-linear input-output behavior, with some hysteresis that is larger during compression than during decompression. An electromechanical model of the sensor needs to be developed to account for this non-linearity.
- Electrical polarization of CNTCS results in signal distortions at low-frequencies that can be eliminated using high-pass filtering (in this paper, above 10 Hz). This may limit applications of the sensing solution to signals with energy concentrated at relatively high frequencies. Here, it was possible to identify a fundamental frequency located around 27 Hz.
- Results of the experimental tests have demonstrated that the output of the cementitious sensors contains the spectral components of all vertical vibration modes identified by off-the-shelf sensors. Non-significant differences were observed between results from the CNTCS and accelerometers.
- The non-linear behavior of the nanocomposite sensors results in harmonic distortion effects that produced a spurious superharmonic frequency equal to the double of the fundamental. This effect could be filtered out via post signal processing.

Acknowledgements

The authors would like to gratefully acknowledge the support provided to this research by the Group of Materials Science and Technology of University of Perugia, coordinated by Professor José M. Kenny, for sharing their knowledge and expertise and for providing materials and equipment for the preparation and analysis of CNTCS. A particular appreciation goes to Dr. Marco Monti, Dr. Maurizio Natali and Dr. Marco Rallini, from the same Research Group, who participated in the development of the CNTCS and in related physical and chemical investigations.

References

[1] Magalhes F, Cunha A, Caetano E. Vibration based structural health monitoring of an arch bridge: from automated oma to damage detection. Mech Syst Signal Process 2012;28:212–28.
[2] Cross E, Manson G, Worden K, Pierce S. Features for damage detection with insensitivity to environmental and operational variations. Proc R Soc A 2012.
[3] Santos JP, Crémona C, Orcesi AD, Silveira P. Multivariate statistical analysis for early damage detection. Eng Struct 2013;56:273–85.
[4] Peeters B, De Roeck G. One-year monitoring of the z24-bridge: environmental effects versus damage events. Earthquake Eng Struct Dyn 2001;30:149–71.
[5] Moaveni B, Behmanesh I. Effects of changing ambient temperature on finite element model updating of the dowling hall footbridge. Eng Struct 2012;43:58–68.
[6] Gentile C, Saisi A. Ambient vibration testing and condition assessment of the paderno iron arch bridge (1889). Constr Build Mater 2011;25:3709–20.
[7] Brownjohn J. Structural health monitoring of civil infrastructure. Philos Trans R Soc A 2007;365:589–622.
[8] Karbhari VM. Encyclopedia of structural health monitoring. Wiley; 2009. p. 1467–76.
[9] Monti M, Natali M, Petrucci R, Kenny J, Torre L. Impact damage sensing in glass fiber reinforced composites based on carbon nanotubes by electrical resistance measurements. J Appl Polym Sci 2011;122:2829–36.
[10] Chiacchiarelli L, Rallini M, Monti M, Puglia D, Kenny J, Torre L. The role of irreversible and reversible phenomena in the piezoresistive behavior of graphene epoxy nanocomposites applied to structural health monitoring. Compos Sci Technol 2013;80:73–9.
[11] Laflamme S, Saleem H, Vasan B, Geiger R, Chen D, Kessler M, Rajan K. Elastomeric capacitor network for strain sensing over large surfaces. IEEE/ASME Trans Mech 2013;18:1647–54.
[12] Laflamme S, Kollosche M, Connor JJ, Kofod G. Robust flexible capacitive surface sensor for structural health monitoring applications. ASCE J Eng Mech 2012;139:879–85.
[13] Materazzi A, Ubertini F, D'Alessandro A. Carbon nanotube cement-based transducers for dynamic sensing of strain. Cem Concr Compos 2013;37:2–11.
[14] Fu X, Chung D. Self-monitoring of fatigue damage in carbon fiber reinforced cement. Cem Concr Res 1996;26:15–20.
[15] Wen S, Chung D. Model of piezoresistivity in carbon fiber cement. Cem Concr Res 2006;36:1879–85.
[16] Meehan D, Wang S, Chung D. Electrical-resistance-based sensing of impact damage in carbon fiber reinforced cement-based materials. J Intell Mater Syst Struct 2010;21:83–105.
[17] Li H, Xiao H, Ou J. Smart concrete, sensors and self-sensing concrete structures. Key Eng Mater 2009;400-402:69–80.
[18] Li G, Wang P, Zhao X. Pressure-sensitive properties and microstructure of carbon nanotube reinforced cement composites. Cem Concr Compos 2007;29:377–82.
[19] Azhari F, Banthia N. Cement-based sensors with carbon fibers and carbon nanotubes for piezoresistive sensing. Cem Concr Compos 2012;34:866–73.
[20] Heeder N, Shukla A, Chalivendra V, Yang S, Park K. Electrical response of carbon nanotube reinforced nanocomposites under static and dynamic loading. Exp Mech 2012;52:315–22.
[21] Konsta-Gdoutos M, Metexa Z, Shah S. Highly dispersed carbon nanotube reinforced cement-based materials. Cem Concr Res 2010;40:1052–9.
[22] Azhari. Cement-based sensors for structural health monitoring, Ph.D. thesis. The University of British Columbia; 2008.
[23] Le K. Time-frequency distributions for crack detection in rotors-a fundamental note. J Sound Vib 2006;294:397–409.
[24] Zonta D, Modena C. Observations on the appearence of dispersive phenomena in damaged structures. J Sound Vib 2001;241:925–33.